Effects of Supersaturation on the Crystal Structure of Gold Seeded III–V Nanowires

ARTICLE *in* CRYSTAL GROWTH & DESIGN · DECEMBER 2008

Impact Factor: 4.89 · DOI: 10.1021/cg800270q

Article

Effects of Supersaturation on the Crystal Structure of Gold Seeded III#V Nanowires

Jonas Johansson, Lisa S. Karlsson, Kimberly A. Dick, Jessica Bolinsson, Brent A. Wacaser, Knut Deppert, and Lars Samuelson

Cryst. Growth Des., **Article ASAP**

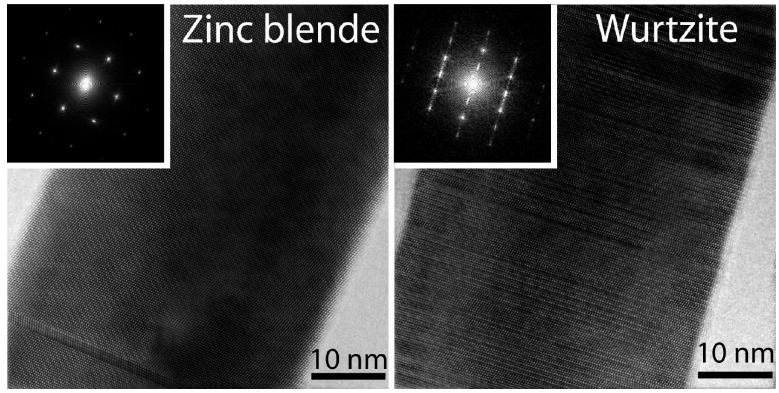

More About This Article

Additional resources and features associated with this article are available within the HTML version:

- Supporting Information
- Access to high resolution figures
- Links to articles and content related to this article
- Copyright permission to reproduce figures and/or text from this article

View the Full Text HTML

Crystal Growth and Design is published by the American Chemical Society. 1155 Sixteenth Street N.W., Washington, DC 20036

CRYSTAL GROWTH & DESIGN
XXXX
VOL. XXX, NO. XX

Effects of Supersaturation on the Crystal Structure of Gold Seeded III−V Nanowires

Jonas Johansson,*,† Lisa S. Karlsson,‡ Kimberly A. Dick,† Jessica Bolinsson,† Brent A. Wacaser,† Knut Deppert,† and Lars Samuelson†

Solid State Physics and the Nanometer Structure Consortium, Lund University, Box 118, SE-221 00 Lund, Sweden, and National Centre for High Resolution Electron Microscopy (nCHREM)/ Polymer & Materials Chemistry, Lund University, Box 124, SE-221 00 Lund, Sweden

Received March 14, 2008; Revised Manuscript Received August 25, 2008

ABSTRACT: We present results that provide fundamental insights on how to experimentally tailor the planar defect density and even the crystal structure in III−V metal particle seeded nanowires, where zinc blende is the stable bulk crystal structure. We have grown GaP nanowires with metal-organic vapor phase epitaxy under different conditions: pulsing of the Ga source, and continuous growth with and without In background. The dominant crystal structure of the nanowires is zinc blende, which when grown under continuous conditions has a high density of twin planes perpendicular to the growth direction. Using pulsed growth, we observed that the twin plane separations were much longer than those observed for continuous growth with an In background. On the other hand, during continuous growth, under In-free conditions, a considerable amount of the wurtzite phase forms. We explain the importance of the In background during growth. With classical nucleation modeling we qualitatively relate the density of planar defects in a nanowire to the growth conditions. For low supersaturations, we predict a low twin plane density, consistent with our experimental observations of pulsed nanowire growth. In addition, we suggest that under certain conditions, it might be possible to grow wires with almost perfect wurtzite structure.

Introduction

During the past decade there has been a tremendous research interest in semiconductor nanowires. These structures can be described as quasi-one-dimensional crystallites, a few micrometers in length and about 5−100 nm in diameter. Nanowires have made a significant impact in applications as diverse as mass sensors, single-electron and tunneling devices, as well as light sources.[1,2]

Metal particle-seeded semiconductor nanowires represent one of the most thoroughly investigated categories of nanowires. In general, the first step is to arrange metal particles on a semiconductor substrate surface. The next step is to insert this sample into a crystal growth chamber. The temperature is then elevated, and the metal particle may form an equilibrium alloy with the substrate. When the growth species are introduced, the metal particle becomes supersaturated, and crystallization of material at the interface between the particle and the substrate initiates. Thus, the nanowire lifts the particle as it grows, with the size of the particle dictating the diameter of the nanowire. The growth continues as long as the concentration of growth species in the ambient phase is high enough to supersaturate the particle. This supersaturation is the driving force for growth. A recent review article discussing nanowire growth mechanisms in greater detail has been written by Kolasinski.[3]

To make efficient use of nanowires in applications it is necessary to be able to control and predict the outcome of a given nanowire fabrication experiment. To do so it is necessary to understand certain fundamental mechanisms of nanowire formation.[3,4] Although more and more knowledge has been gained in recent years, a solid theoretical description for metal particle-seeded nanowire formation is still missing. One of the most general attempts has been formulated by Dubrovskii et al.[5] Their model includes and unifies several different kinetic pathways, such as adsorption, surface diffusion, and nucleation, any one of which can be rate limiting, depending on the growth conditions.

Still, many effects concerning the formation of nanowires remain unresolved. One such example is the zinc blende−wurtzite polytypism found in many III−V semiconductor nanowires for which zinc blende is the stable crystal structure in bulk material. Although this problem has been discussed by several researchers, we note that two of the most interesting and pioneering approaches have been taken by Akiyama et al.[6] and Glas et al.[7]

Akiyama et al. assume a realistic hexagonal wire shape, where the wire is bounded by {110}-like side walls. They calculate the total energy of the wire by means of Khor−Das−Sarma type empirical potentials. This atomistic approach allows the authors to compare the energy of pure wurtzite and pure zinc blende nanowires with different thicknesses. The authors propose a cross-over wire diameter, below which wurtzite is the stable structure and above which zinc blende is the stable structure.[6] One problem with this approach is that the calculated cross-over thickness is around 15−20 nm, while there is clear experimental evidence of wurtzite wires considerably thicker than this for the materials considered.[8]

The approach of Glas et al. is based on classical nucleation theory. Using different surface energies for zinc blende and wurtzite and the inclusion of a certain interface energy for the wurtzite nucleus, they determine that the nucleation barriers for zinc blende and wurtzite should be different. This in turn leads the authors to propose certain experimental conditions (in terms of supersaturation) where wurtzite or zinc blende will be favorable.[7]

Although these approaches are different in nature, we note an interesting similarity, which is based on the underlying physics. For the same material, the surface energies of the wurtzite structure can, at least in some cases,[9] be lower than those of zinc blende, whereas the bulk contribution to the total

* To whom correspondence should be addressed. E-mail: jonas.johansson@ftf.lth.se.
† Solid State Physics and the Nanometer Structure Consortium.
‡ National Centre for High Resolution Electron Microscopy (nCHREM)/ Polymer & Materials Chemistry.

10.1021/cg800270q CCC: $40.75

energy is higher for wurtzite (for materials where zinc blende is the stable bulk crystal structure).

The purpose of the current investigation is to test a hypothesis on how to experimentally modulate the crystal structure of metal particle-seeded nanowires. A few years ago, it was observed that for GaAs nanowires grown by chemical beam epitaxy, the crystal structure of the part of the wire directly under the gold particle depends on the cooling conditions.[10] If both the Ga and the As supplies were switched off before cooling down, the result was a nanowire with mostly wurtzite structure, but with a high density of stacking faults. If only the Ga supply was switched off and the cooling was performed under As supply, a neck region under the gold particle formed during cooling down. The neck region showed the zinc blende crystal structure and only very few twin planes[10] (see also ref 7 for a similar observation for MBE GaAs nanowire growth). It is expected that this neck region forms during cooling as the remaining Ga in the particle combines with As from the supply; this growth will not occur when both supplies are switched off.

The significant difference in crystal structure observed using different cooling conditions is tentatively attributed to the influence of supersaturation during growth. At high supersaturation we expect a high density of twin planes and potentially also wurtzite formation (in materials where zinc blende is the bulk crystal structure). Correspondingly, at low supersaturation (such as during cooling) we expect pure zinc blende structure with only a few twin planes. Thus, by pulsing the Ga supply one would expect a periodically recurring low supersaturation during the Ga off times, which would result in wires with few twin planes. In the current investigation we test this hypothesis about the influence of supersaturation on the crystalline properties of metal particle-seeded III−V nanowires.

To demonstrate this effect we grow gold-particle-seeded GaP nanowires with metal-organic vapor phase epitaxy (MOVPE). We investigate different growth conditions, such as pulsed or continuous Ga supply and In-containing or In-free background. As a result, we find that the density of twin plane defects and the amount of wurtzite in these zinc blende nanowires can be tuned. Like Glas et al.,[7] we interpret our results using classical nucleation theory. Taking nucleation probabilities into consideration, we demonstrate that the density of twin planes and the amount of wurtzite in the wires is a strong function of the growth conditions. Furthermore, our qualitative modeling offers an explanation for the formation of wurtzite nanowires in materials where the bulk crystal structure is zinc blende.

Although we use gold-particle-seeded GaP nanowires to demonstrate this effect, our results are of general nature and should also apply to other metal-seeded III−V nanowires with zinc blende as the bulk crystal structure, such as InP and GaAs.

Experimental Procedures

Size-selected gold aerosol particles[11] with a nominal diameter of 40 nm were deposited onto GaP (111)B substrates at an approximate surface density of one particle per micrometer^2. After gold deposition, the substrates were transferred to a low-pressure MOVPE reactor. Before growth, the gold-particle-strewn samples were annealed under a phosphine-containing hydrogen flow of 6 L/min at 650 °C for 10 min. After this, the temperature was ramped down to a growth temperature of 470 °C and trimethyl gallium (TMG) was introduced to initiate growth. The total pressure in the reactor was 100 mbar. The molar fractions of phosphine and TMG in the flowing gas were 7.5×10^{-3} and 1.25×10^{-5}, respectively (V/III ratio 600). The reason for the high V/III ratio is the inefficient cracking of PH_3 at our relatively low growth temperatures.

The samples were grown in two different ways, which we refer to as *continuous* and *pulsed* growth. In the continuous case, the wires were grown for 4 min. The TMG was then turned off, and the samples were cooled in a phosphine atmosphere. In the pulsed case, the growth was initiated by 1 min growth under continuous conditions, and then the TMG source was turned off for 1 min, then turned on again for 10 s. After 20 such pulses, the sample was cooled down under phosphine (as in the continuous case). A schematic depiction of the pulsed growth technique is shown in Figure 1. We grew continuous and pulsed samples with two different graphite susceptors: one indium-contaminated (from previous growths of In-containing materials) and one that had only been used under indium-free conditions. Growth with an In-contaminated susceptor gives rise to a slight In background in the reactor, and In is readily dissolved in the gold particles. We will refer to these two conditions as growth with In background and with In-free background, respectively.

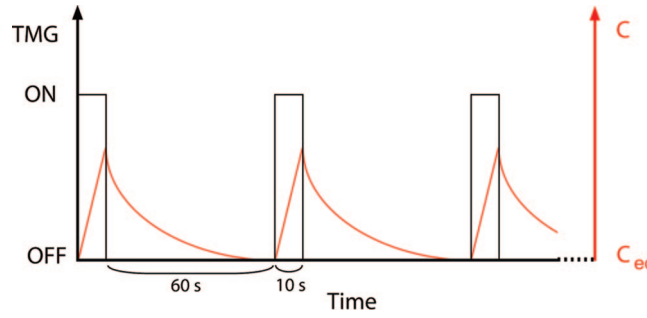

Figure 1. Schematic depiction of the pulsing. The left *y*-axis indicates the state of the TMG. ON means that TMG is sent to the growth chamber while OFF means that it is sent to the bypassing vent line. The pulses consist nominally of 60 s OFF and 10 s ON. This pattern is repeated 20 times during pulsed growth. The right *y*-axis (red) indicates the Ga concentration in the seed particles. The red curves indicate the trends in the Ga concentration during pulsed growth. When the TMG is turned ON, the Ga concentration increases in the seed particles. When the TMG is turned OFF, the Ga concentration decreases toward the equilibrium concentration, since it is consumed by the growing nanowires.

Since our growth experiments are carried out in a cold-wall reactor, the susceptor acts as the primary source of contamination during growth. However, other parts of the reactor may give rise to trace In-contamination, as will be shown later in this investigation. Also note that our background amounts of In dissolves in the Au particles but is not found in the nanowires (within the energy dispersive X-ray spectroscopy detection limit).

To estimate the growth and equilibrium Ga and In concentrations in the alloy particles, we also grew samples under continuous conditions that were cooled down in H_2 only (rather than PH_3 and H_2).[12]

Scanning electron microscopy (SEM) was used to obtain overview images of the nanowire samples. The images were acquired with the electron beam of a combined focused ion beam and SEM instrument, FEI Nova NanoLab 600, at an acceleration voltage of 10 kV.

High resolution transmission electron microscopy (HRTEM) images were used to determine the structural nature of the nanowires, both in terms of overall crystal structure and imperfections such as twin planes. The HRTEM images were acquired with a 300 kV field emission gun TEM from JEOL Ltd., Japan. Deposition of the nanowires onto carbon film coated Cu grids was performed by gently rubbing the grid against the sample, in most cases cutting the nanowires off at the base. The orientation of the nanowires in the field of view was determined from corresponding diffraction patterns and Kikuchi poles.[13] Energy dispersive X-ray spectroscopy (EDS) was used in scanning transmission electron microscopy (STEM) mode to measure the Ga and In concentrations in the alloy particles.

Nanowire Growth Results

In Figure 2, we show an overview SEM image of a GaP nanowire sample grown under continuous conditions and In background. It shows that the wires are only slightly tapered and have a length in the micrometer range. The areal density of nanowires and their diameters are determined by the density

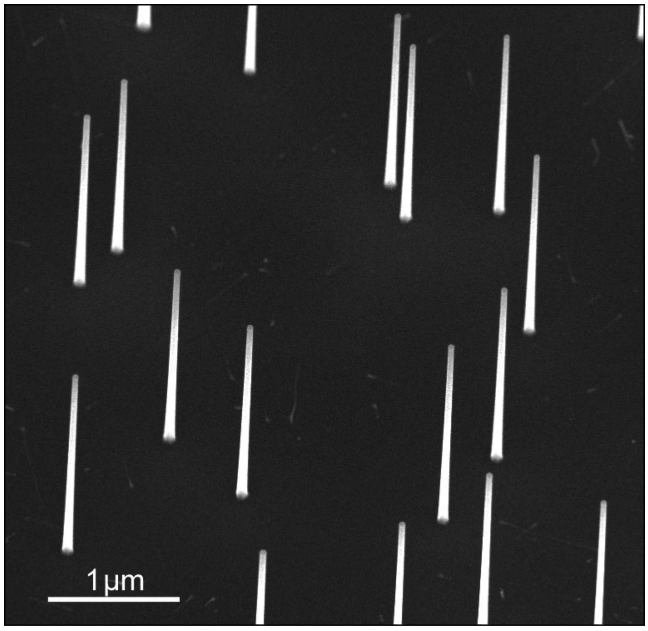

Figure 2. Overview SEM image, with a tilt angle of 30°, of a sample grown under continuous conditions with In background.

and sizes of the gold alloy particles. The overall nanowire sample morphology shown in Figure 2 is representative of all investigated growth conditions.

We have previously shown that MOVPE-grown gold-particle-assisted GaP nanowires have zinc blende crystal structure, with a high density of twin planes perpendicular to the ⟨111⟩B growth direction.[14] The twin segments are of truncated octahedral shape and limited by {111} facets. This gives rise to a situation where sidewalls with an overall orientation of {112} consist of alternating {111}A and {111}B microfacets. The segment thicknesses follow exponential distributions, which shows that there is a certain probability of twin plane formation, independent of segment thickness (within a certain range). The thicknesses of the segments decrease with increasing temperature.[14]

At this point it is suitable to recall that in the ⟨111⟩ direction the zinc blende stacking sequence can be schematically represented by AaBbCc. Each pair of upper and lower case letters correspond to specific atomic planes, which consist of molecular units arranged so that group III and group V atoms are vertically aligned and separated by one bond length; see Figure 3a.[15] Without loss of generality we will refer to this stacking sequence as ABCABC stacking. The stacking sequence in the corresponding direction in wurtzite, the ⟨0001⟩ direction, can be represented by ABAB. Nucleation of a fault plane, such as a B plane on top of ABC in zinc blende, resulting in ABCB (Figure 3b and 3c), occurs readily at typical nanowire growth conditions. The extra interface energy associated with this is the twin plane energy, which is commonly approximated by half of the stacking fault energy.[16]

We have chosen to refer to this situation as *fault plane* nucleation instead of twin plane nucleation because it is impossible to tell at this stage of formation whether the specific plane will become a twin plane or the first plane in a wurtzite segment. Thus, if a zinc blende stacking sequence continues on top of this plane, a twin is created. The stacking sequence is then mirrored around the first C plane resulting in ABCBAC (Figure 3b). If on the other hand a new fault plane is nucleated on top of ABCB resulting in ABCBC (Figure 3c), wurtzite is starting to form. We count the specific situation of ABCBC as two layers of wurtzite on top of three layers of zinc blende. Thus, the formation of n fault planes in a sequence results in an n monomolecular layer (ML) thick wurtzite segment, just as the formation of n ordinary planes in a sequence, before the nucleation of a fault plane, gives an n ML thick zinc blende segment.

With this in mind we return to the present results. In Figure 4, we display HRTEM images of sections of wires grown under different conditions: Figure 4a − pulsed growth, In background; Figure 4b − continuous growth, In background; Figure 4c − continuous growth, In-free background. From these figures it is easy to observe that the wires grown under different conditions differ considerably in crystal structure. The wires grown under pulsed conditions (Figure 4a) have significantly longer twinning segments than the wires grown under continuous conditions (Figure 4b). The longest segment in the wire in Figure 4a is 200 ML and the average segment is 20 ML thick. The average twin segment for the wire in Figure 4b is 3.5 ML. The wire in Figure 4c has the same characteristics as the one in Figure 4b, but has in addition extended wurtzite segments. The longest wurtzite segment observed in the wire in Figure 4c is 21 ML thick and the average wurtzite segment is 3.5 ML. On the other hand, no such extended wurtzite segments were found in the wires grown under conditions such as those in Figure 4b. The diffraction pattern insets in Figures 4a and c show that the crystal structure of the part of the wire in Figure 4a is zinc blende in one of its twin orientations, and that wurtzite segments extended enough to show wurtzite diffraction characteristics appear in the wire in Figure 4c.

It should be noted here that growth under different conditions also affects the axial growth rate of the wires. The wires grown under pulsed conditions with In background (Figure 4a) are on average 4.3 μm long. The wires grown under continuous conditions with In background (Figure 4b) are 2.7 μm and without In background (Figure 4c) they are 3.0 μm.

In this investigation we attempted to vary the supersaturation in two different ways: *pulsed or continuous growth* and *In background or In-free background*. During pulsed growth, when the TMG is switched off, the Ga concentration decreases in the alloy particle, while the nanowire continues to grow (this is similar to what happens during cooling if the As supply is left on). After a while, when the Ga concentration approaches the equilibrium concentration, the growth should cease.

From our nanowire length measurements and growth times (see Experimental Procedures) we estimate that the nanowires grow by approximately 70 nm during one Ga off-period. This is a nominal value, which is based on 10 s Ga on-periods, and is certainly too large. However, the Ga precursors linger at the substrate surface a few seconds after the Ga has been switched off, which *effectively* could make the Ga on-periods a few seconds longer. For an effective Ga on-time between 15 and 16 s we would instead get 10 nm GaP nanowire growth during the Ga off-periods, just by emptying the particle of Ga. This is fully reasonable and in accordance with the observations of GaAs growth in the CBE.[10]

When the TMG is switched back on, the Ga concentration in the alloy particle will increase; see schematics in Figure 1. Thus, by using pulsed growth conditions we should be able to reach very low supersaturations during the Ga off periods. We also note that one could vary the pulse lengths to control the maximum supersaturation during pulsing. This effect was, however, not investigated.

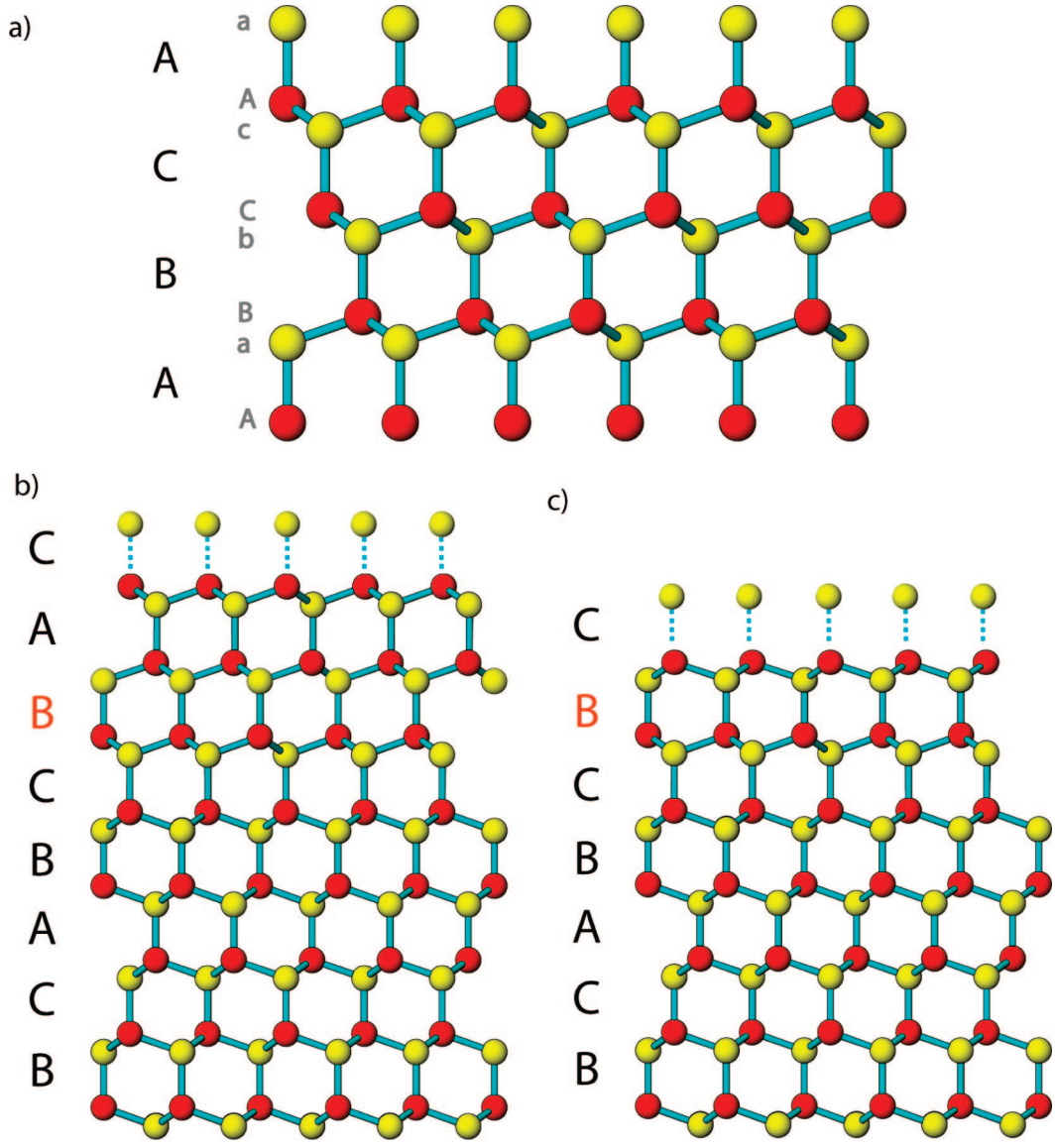

Figure 3. 2D projections in the $\langle \bar{1}10 \rangle$ viewing direction of possible stacking sequences during nanowire growth. In (a) zinc blende stacking is shown. In (b) and (c) the first fault plane on top of a zinc blende region is indicated in red. If the stacking sequence continues with layer A and C as in (b), a twin segment is forming and the stacking sequence is mirrored around the C layer under the fault plane. If on the other hand, another fault plane forms on top of the red-marked B layer as in (c), wurtzite phase starts to form.

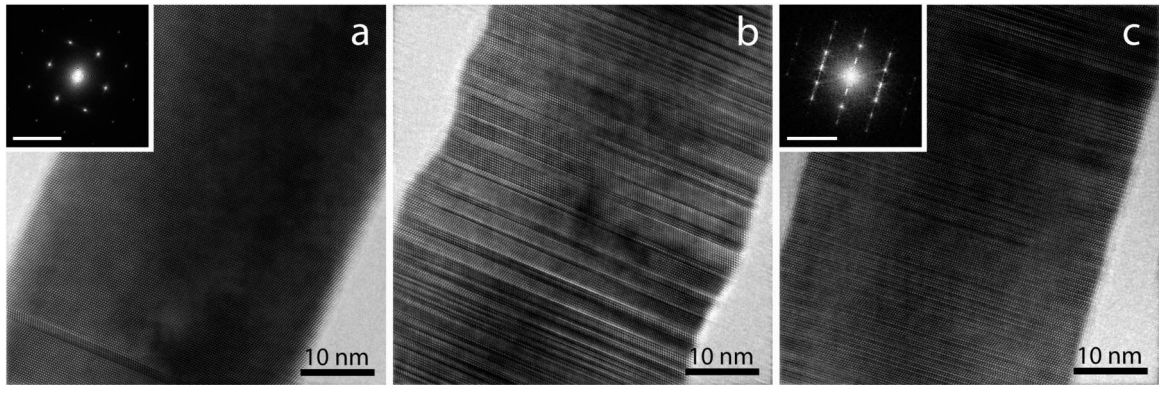

Figure 4. HRTEM images of parts of GaP nanowires. The wire in (a) is grown under pulsed conditions, the wire in (b) under continuous conditions with In background, and the wire in (c) under continuous conditions with In-free background. The diffraction pattern insets in (a) and (c) show zinc blende and wurtzite characteristics, respectively. The scale bars in the insets correspond to 5 nm^{-1}.

When growing nanowires under In-rich conditions, In from the background is readily dissolved into the alloy particles, and remains there. This decreases the Ga solubility of the particles and might decrease the obtainable supersaturation during

Table 1. In and Ga Content in the Au Seed Particles As Measured with EDS[a]

	In background		In free background	
	H_2	PH_3	H_2	PH_3
In (at %)	20 −30	20 − 30	0 − 5	0 − 5
Ga (at %)	0	0	20 −26	0

[a] Nanowire samples were grown with and without In background. The growth was terminated in two different ways: H_2 refers to cooling in H_2 only, whereas PH_3 refers to cooling in a PH_3 containing H_2 flow. The value 0 means that the concentration is below the detection limit which is about 3 atomic percent (at %).

nanowire growth compared to growth under In-free conditions. To test this effect we have compared the Ga concentration in the alloy particles in samples that were cooled down in PH_3 with samples that were cooled down in H_2. The effect of replacing PH_3 with H_2 before cooling down is that the wires cease to grow, as there is a lack of group V material. The Ga in the particle is expected to remain, and its concentration can be measured after growth and cooling down. The measured concentration is then an estimation of the growth concentration of Ga in the particle.[12]

The samples cooled down the conventional way, under PH_3, continue to grow until the Ga concentration in the alloy particle reaches the equilibrium concentration.

In Table 1, the results of the EDS concentration measurements are summarized. Here it is shown that when growing with an In background concentration, the gold alloy particles contain an In concentration of 20−30 atomic percent (at %). Since In from previous growth experiments can linger in the reactor for a long time, we detect a few at % In in the particle even when we grow at nominally In-free conditions, that is with an In-free susceptor. When growing with In background, the Ga growth concentration and the Ga equilibrium concentration are both below the detection limit of the EDS setup, which is around 3 at %. With In-free background, the Ga growth concentration is at least 20 at %, whereas the equilibrium concentration is below 3 at % (see Table 1). No P was detected in particles on any of the samples. From these measurements we conclude that the presence of In decreases the solubility of Ga in the alloy particle. By comparing the Ga growth concentrations for the two cases, we also conclude that the supersaturation is higher for growth under In-free conditions, since the Ga equilibrium concentration is less than 3 at % in both of these cases. It should be noted that no In was detected in the GaP nanowires (within the detection limit), even when they were grown with In background.

One could argue that an easier way to increase the supersaturation would be to increase the TMG flow. This would undoubtedly lead to an increased supersaturation in the entire growth system. In the extreme case this could have the opposite effect, since it could lead to increased competition from direct deposition from the vapor resulting in substrate growth and growth on the wire sidewalls leading to tapering. In such a case, the group III material available for wire growth could be less than with a lower group III flow, resulting in a lower supersaturation at the wire growth interface. By our approach, that is, altering the seed particle, only the local supersaturation above the nanowire growth interface is expected to change.

Nucleation Model

We develop here a model based on classical nucleation theory to explain the abundance of twin planes and the formation of wurtzite in metal particle-assisted nanowires of III−V materials with zinc blende as bulk crystal structure. The growth results

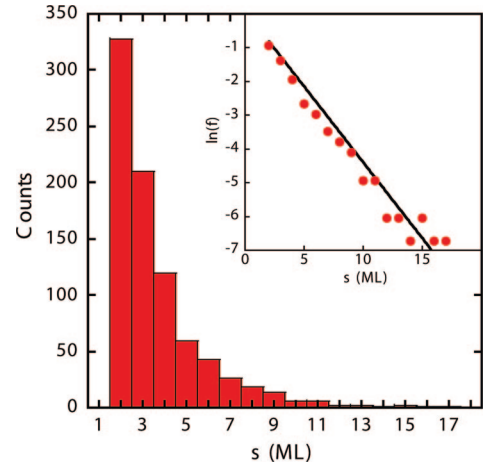

Figure 5. Histogram of segment thicknesses for a wire grown at continuous conditions with In background. In the inset the natural logarithm of the segment thickness frequency is plotted on the *y* axis and the segment thickness on the *x* axis. The solid line is a least-squares fit to the exponential distribution, eq 1.

described above (Figure 4) will be discussed in view of this model to better understand the nanowire microstructure. To develop this model we must first make two assumptions: (i) The nanowires grow layer-by-layer by monocenter nucleation at the edge of the nanowire−Au interface (the three phase boundary). (ii) The nucleation can be described by a Poissonian process.

Assumption (i) is discussed and justified in ref 14 and also by Davidson et al.[17] Assumption (ii) means that the number of nucleation events in non-overlapping time intervals is statistically independent. In other words, the process is memory-less. In such a process, the distribution of waiting times between successive events is exponential, or in the discrete case, geometric. Thus, the waiting times between successive twin plane nucleation events should also be exponentially distributed (but on a longer time scale), leading to geometrically distributed twin segment lengths. In Figure 5, we show a histogram of segment lengths for a sample grown under continuous conditions with In background. The inset shows a fit of the segment thickness frequency to the exponential distribution,

$$f(s) = \frac{1}{\alpha}\exp\left(-\frac{s-\beta}{\alpha}\right) \qquad (1)$$

In eq 1, s is the segment thickness, α is the scale parameter, and β is the location parameter, which we set equal to 2, since no segment is thinner than 2 ML.[14] The average segment thickness is given by $s_m = \alpha + \beta$, according to the properties of the exponential distribution. The excellent agreement of the least-squares fit of eq 1 to the experimental data (Figure 5, inset), with α as the only fitting parameter, shows that the segment thicknesses are indeed geometrically distributed (in this case with $s_m = 4.2$ ML) and assumption (ii) is justified. It should also be noted that Poissonian nucleation is one of the cornerstones in the Kolmogorov−Johnson−Mehl−Avrami nucleation model.[18−22]

Having justified these assumptions we are now ready to develop our model, describing nucleation of both ordinary and fault planes. Because of the qualitative nature of our model, the exact shape of the nucleus is not crucial. Since the nucleation occurs at the nanowire edge,[14,23] it is natural to assume that the two-dimensional nucleus has a semicircular shape; see Figure 6. Other shapes have also been considered; Glas et al. used a

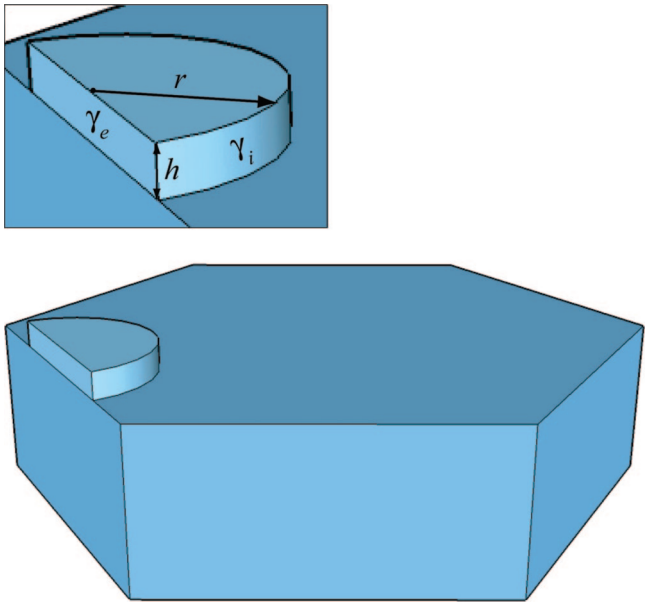

Figure 6. Schematic illustration of the nucleation geometry. The bottom figure is a schematic view of the two-dimensional, semicircular nucleus on top of the nanowire, coinciding with the edge. The top figure is a magnification of the nucleus, indicating the symbols used in eqs 2 and 4.

triangular nucleus in their model.[7] For the semicircular geometry the Gibbs free energy for nucleation[24] reads,

$$\Delta G(r) = -\frac{\pi}{2} r^2 \Delta\mu + \frac{\pi}{2} r^2 \sigma + r\Gamma \tag{2}$$

where r is the radius of the nucleus, $\Delta\mu$ is the chemical potential per area unit, σ is the energy of the interface between the nucleus and the underlying layer, and Γ is the step energy contribution. The chemical potential is given by

$$\Delta\mu = \frac{k_B T}{s_c} \ln \frac{C}{C_{eq}} \tag{3}$$

where k_B is Boltzmann's constant, T is the absolute temperature, and C and C_{eq} are the Ga concentrations in the alloy particle during nanowire growth and at equilibrium, respectively. Since the phosphorus has extremely low solubility in gold[25] and is thus expected to arrive at the growth interface from the vapor phase where it is in excess, we omit it from the model. The parameter, s_c, is the area of an atomic site at the growth interface. For a zinc blende {111} surface, this quantity is given by

$$s_c = a^2\sqrt{3}/4$$

where a is the lattice parameter. The interface energy σ in eq 2 is zero for an ordinary plane and equal to the twin plane energy, $\sigma = \sigma_f$, for a fault plane. The step energy can be written as

$$\Gamma = h(\pi y_i + 2y_e) \tag{4}$$

where

$$h = a/\sqrt{3}$$

is the height of the 1 ML thick nucleus and the parameters y_i and y_e are the specific step energies of the inner part of the nucleus under the gold (subscript "i" for inner) and of the part of the nucleus along the three phase boundary (subscript "e" for edge), respectively. The nucleation geometry and the notation in eq 2 and 4 are schematically outlined in Figure 6.

The energy barrier for nucleation is given by the maximum value of ΔG and the corresponding r value, r^*, is the critical size of the nucleus. Differentiating eq 2, setting the result to zero, $\partial\Delta G/\partial r = 0$, and solving for r gives,

$$r^* = \frac{\Gamma}{\pi(\Delta\mu - \sigma)} \tag{5}$$

Inserting eq 5 into eq 2 and explicitly considering both the ordinary and the fault nucleus, we get the energy barriers for the two cases of nucleation:

$$\Delta G^* = \frac{\Gamma^2}{2\pi\Delta\mu} \tag{6}$$

and

$$\Delta G_f^* = \frac{\Gamma_f^2}{2\pi(\Delta\mu - \sigma_f)} \tag{7}$$

where ΔG^* is the ordinary nucleation barrier and ΔG_f^* is the fault plane nucleation barrier. In eq 7 we see that for a fault plane to nucleate, the chemical potential has to overcome the twin plane energy, $\Delta\mu > \sigma_f$. Moreover, for fault plane nucleation to be energetically favorable, and thus ultimately for the wurtzite structure to form, the energy barrier for fault plane nucleation must be smaller than the barrier for ordinary plane nucleation:

$$\Delta G_f^* < \Delta G^* \tag{8}$$

This inequality is satisfied if the step energy of the fault nucleus is smaller than the step energy of the ordinary nucleus and if the chemical potential is larger than a certain value dependent on the ratio between the step energies, $\Gamma_f^2\Delta\mu < \Gamma^2(\Delta\mu - \sigma_f)$.

The step energies of the ordinary and fault nucleus are not known experimentally and therefore have to be estimated. We approximate the inner and edge step energies to be equal for the ordinary nucleus, $y_i = y_e$, and we assume that the inner step energies for the two different nuclei are equal, $y_i^f = y_i$. Further, the edge step energies are closely related to the surface energies and should follow the same trends when the structure changes from zinc blende to wurtzite. Therefore, one can argue that the edge step energy for the fault plane, y_e^f, should be lower than the edge step energy of the ordinary plane, y_e. Thereby their ratio is smaller than one, $f = y_e^f/y_e < 1$. On the basis of this discussion and the assumption of a semicircular nucleus (Figure 6), we can rewrite the condition for fault plane preference (eq 8) as

$$\Delta\mu > \sigma_f \frac{(2+\pi)^2}{4(1-f)(1+\pi+f)} \tag{9}$$

We will soon see that this relationship is a necessary, but not sufficient, condition for wurtzite formation in nanowires with zinc blende as bulk crystal structure.

The next step is to estimate nucleation probabilities for ordinary and fault plane nucleation. We note that the nucleation rates for ordinary and fault plane nucleation are proportional to $\exp(-\Delta G^*/k_B T)$ and $\exp(-\Delta G_f^*/k_B T)$, respectively. Following the approach in ref 14 the fault plane nucleation probability is given by,

$$p_f = \frac{\exp(-\Delta G_f^*/k_B T)}{\exp(-\Delta G^*/k_B T) + \exp(-\Delta G_f^*/k_B T)} \tag{10}$$

Thus, the probability for ordinary plane nucleation is given by, $p = 1 - p_f$.

Discussion

In Figure 7, we plot p_f, given by eq 10, as a function of the chemical potential, $\Delta\mu$, for five different ratios between the edge

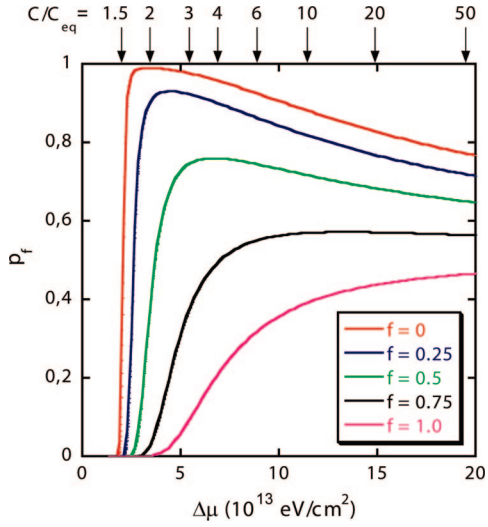

Figure 7. Fault plane nucleation probability as a function of the supersaturation. The chemical potential is shown on the bottom x axis, and the supersaturation ratio is shown on the upper x axis. The solid curves account for different values of the ratio, f, between the edge step energy of a fault nucleus and of an ordinary nucleus.

energies $f = 0$, 0.25, 0.50, 0.75, and 1. To do so, we assume that the nuclei have a thickness of 1 ML (in the ⟨111⟩ direction), $h = a\sqrt{3}/3$ with $a = 5.45$ Å (the lattice parameter of GaP). Following Voronkov[26] and Hurle,[27] we estimate the step energy of zinc blende GaP as $y = 7.8 \times 10^{13}$ eV/cm^2, using the expression for a Kossel crystal. The twin plane energy is roughly half the stacking fault energy, which is 41×10^{-7} J/cm^2 (ref 28), that is, $\sigma_t = 1.3 \times 10^{13}$ eV/cm^2. On the upper x axis, the supersaturation ratio, C/C_{eq}, which is related to $\Delta\mu$ by eq 3, is shown.

It can be seen in Figure 7 that the fault plane nucleation probability as a function of chemical potential first increases toward a maximum and then decreases and tends to $p_f = 1/2$ for high, possibly unreasonable, values of $\Delta\mu$. Formally, increasing the temperature would have the same smearing effect on the statistics. However, many of the relevant parameters might have temperature dependencies which are not well understood, so our model does not enable us to draw any conclusions in the high temperature limit. The probability maximum is most narrow and highest for low f values, that is, when the ratio between the surface energy of wurtzite and zinc blende is vanishing. For higher f values the maximum value of p_f is lower and the curve around the maximum is flatter as compared to that for low f values. When f reaches one, the curve monotonically approaches $p_f = 1/2$ from below.

The nucleation probability itself is a magnitude that is hard to measure. Therefore we will take advantage of the geometrical distribution of segment thicknesses (see Figure 5). According to the properties of the geometric distribution, the probability distribution of nucleating exactly k fault planes in a sequence, that is, a k ML thick wurtzite segment, before an ordinary nucleus forms is given by $p_f^k(1 - p_f)$, $k = 0, 1, 2, \ldots$ and the average wurtzite segment thickness (the average value of k) is given by,

$$s_{WZ} = p_f/(1 - p_f) \tag{11}$$

Since we cannot characterize a segment thinner than two ML, we require that $p_f > 2/3$ to actually have wurtzite segments with average thickness, s_{WZ}, of two or more ML in a nanowire. As two examples we note that for average wurtzite segments thicker than 10 ML p_f needs to be larger than 0.91, and for $s_{WZ} > 100$ ML, we require that $p_f > 0.99$. By combining eqs 10 and 11, we can pose a stronger condition than eq 8 for wurtzite to form, thus relating the difference in nucleation barriers to the average wurtzite segment thickness observed in a nanowire

$$\Delta G_f^* + k_B T \ln s_{WZ} < \Delta G^* \tag{12}$$

It is interesting to note that eq 7 is a necessary but not sufficient condition for wurtzite structure formation, since it corresponds to $s_{WZ} > 1$, which only indicates an increased probability of fault plane formation. In this case, the probability of forming several fault planes in a sequence, that is, wurtzite structure, can still be vanishingly low.

The above reasoning can of course be turned around, so that for low supersaturation, $p_f < 1/2$, we can formulate a law similar to eq 12, relating the difference in nucleation barriers to an average zinc blende segment thickness, s_{ZB}. This is left to the reader. Here we are satisfied by noting that $s_{ZB} = (1 - p_f)/p_f$ so that, for example, $s_{ZB} > 2$ ML corresponds to $p_f < 1/3$, $s_{ZB} > 10$ ML corresponds to $p_f < 0.09$, and $s_{ZB} > 100$ ML corresponds to $p_f < 0.01$.

Before discussing our nanowire growth results (Figure 4) in view of the nucleation model presented in Figure 7, it is of interest to comment on reasonable ratios, f, between the edge step energies of the wurtzite and zinc blende phases. Because of the lack of step energy data in the literature, we estimate reasonable f ratios by comparing surface energy data for zinc blende and wurtzite phases of the same materials. There does not seem to be much data here either, but we have found data for ZnS, which can be stable in either phase depending on the temperature.[9] Zhang et al. estimate average surface energies for zinc blende ZnS nanoparticles with {100}, {110}, and {111} facets to be 0.86 J m^{-2}. The corresponding average surface energy for wurtzite ZnS nanoparticles is 0.57 J m^{-2}.[9] This leads to $f = 0.57/0.86 \approx 0.66$. This gives a hint that f values between 0.5 and 1 could be realistic. However, for specific orientations or under certain conditions, it is possible that f is considerably lower.

We are also aware of that the step energies could vary with the composition of the seed particle. As the surface energy of In is approximately a factor of 2 smaller than that of Au (see surface energy values in ref 29 for In and ref 30 for Au), the step energies of the nuclei are probably smaller when the seed particle contains In than when it is In-free. Thus, we expect slightly lower nucleation barriers, ΔG^* and ΔG_f^*, for growth with In background but virtually no effect on the fault plane nucleation probability, p_f. Because of the qualitative nature of our model and the expected smallness of this effect we safely omit it from our calculations.

How do our experimental results fit into this growth model? As previously described, the samples shown in Figure 4 were grown under three different conditions: *pulsed* (Figure 4a), *continuous* (Figure 4b), and *continuous In-free* (Figure 4c). The resulting zinc blende or wurtzite average segment thicknesses (see description of Figure 4 above) can be related to p_f by eq 11 so that for the pulsed sample $p_f = 0.05$, for the continuous one $p_f = 0.22$, and for the continuous In-free sample $p_f = 0.78$. On the basis of the $f = 0.5$ curve in Figure 7, we estimate that the pulsed sample was grown at a supersaturation ratio, $C/C_{eq} \approx 1.5$. Since this is based on the average segment length, we regard this value as an upper limit. During pulsing, when the TMG is switched off, even lower supersaturations may be reached, possibly $C/C_{eq} \rightarrow 1$, leading to much longer zinc blende segments, see Figure 4a. For the continuous growth $C/C_{eq} \approx 2$ and for the sample grown under In-free conditions $C/C_{eq} > 3$. These values follow the expected supersaturation trend and qualitatively justify our nucleation model.

In addition, as the growth rate should increase with increasing supersaturation, the observation that the wires grown under In-free conditions are slightly longer than the wires grown with In background can also be explained by the higher supersaturation in the In-free case.

Quantitatively, we are not able to draw any conclusions on the exact supersaturations, since we do not know the f ratio. In our comparison we used the most realistic curve for our situation, that is, the one with the highest f value having a maximum above $p_f = 0.7$. Moreover, we have assumed that the step energy of the part of the nucleus inside the metal particle is the same for an ordinary and a fault nucleus. This is only a first approximation; a difference of the inside step energies would shift the curves to higher p_f maxima.

To conclude, our findings show that the density of planar defects (twin planes and stacking faults) and ultimately the probability of wurtzite formation in III−V zinc blende nanowires are determined by the thermodynamic nucleation conditions. The main parameters that influence these conditions are the supersaturation and the ratio between the step energies of a fault step and an ordinary step. Of these two parameters, only the supersaturation can be regarded as an experimental control parameter. The step energies are instead determined by the materials combination—the semiconductor and the seed particle metal. These two parameters act together, and as rules of thumb we note that the wurtzite structure can be achieved when the step energy ratio is small and the supersaturation is fairly high, see Figure 7. Nanowires with zinc blende structure are instead achieved at low supersaturations.

The introduction of pulsed growth enables us to reach very low supersaturations. The composition of the seed particles also has an impact on the supersaturation. When growing nanowires under In-rich conditions, In from the background is readily dissolved into the Au seed particles. This decreases the Ga solubility of the particles and has a decreasing effect on the supersaturation during nanowire growth compared to growth under In-free conditions.

Although the experimental results are limited to GaP, our results are of a general nature and should also apply to nanowires of other III−V materials with zinc blende bulk crystal structure, such as InP and GaAs. Indeed, preliminary results show that gold-particle-seeded GaAs nanowires grown under pulsed conditions have significantly longer zinc blende segments than those grown under continuous conditions.

Conclusions

We have grown gold-particle-seeded, ⟨111⟩B-oriented GaP nanowires with metal-organic vapor phase epitaxy (MOVPE). We investigate growth under pulsed conditions where the Ga source is periodically switched on and off, as well as continuous growth, with and without indium background. The nanowires have zinc blende crystal structure but have a high density of fault planes perpendicular to the growth direction. Depending on the stacking sequence around the fault plane it can either be a twin plane or part of a wurtzite segment. When pulsed growth conditions are used, the fault plane density is low, leading to extended zinc blende twin segments, up to 100−200 monomolecular layers (ML) thick. For continuous growth with In background, the fault plane density is higher, leading to average zinc blende segments of 3−4 ML. Finally, for continuous growth under In-free conditions, the fault plane density is so high that we observe wurtzite segments, that is, several fault planes in a sequence on average 3−4 ML thick. We demonstrate that the supersaturation increases as we go from pulsed growth to continuous growth with In to continuous In-free growth.

By introducing a classical nucleation model including nucleation statistics, we are able to relate the fault or twin plane density in a nanowire to the experimental growth conditions, and also to explain the occurrence of wurtzite in nanowires where zinc blende is the stable bulk crystal structure.

Acknowledgment. This work was carried out within the Nanometer Structure Consortium in Lund and was supported by grants from the Swedish Research Council (VR), the Swedish Foundation for Strategic Research (SSF), the IP NODE (EU contract nr 015783 NODE), and the NoE SANDiE (EU contract nr NoE500101-2).

References

(1) Fan, H. J.; Werner, P.; Zacharias, M. *Small* **2006**, *2*, 700–717.
(2) Thelander, C.; Agarwal, P.; Brongersma, S.; Eymery, J.; Feiner, L. F.; Forchel, A.; Scheffler, M.; Riess, W.; Ohlsson, B. J.; Gösele, U.; Samuelson, L. *Mater. Today* **2006**, *9*, 28–35.
(3) Kolasinski, K. W. *Curr. Opin. Solid State Mater. Sci.* **2006**, *10*, 182–191.
(4) Law, M.; Goldberger, J.; Yang, P. D. *Annu. Rev. Mater. Res.* **2004**, *34*, 83–122.
(5) Dubrovskii, V. G.; Sibirev, N. V.; Cirlin, G. E.; Harmand, J. C.; Ustinov, V. M. *Phys. Rev. E* **2006**, *73*, 021603.
(6) Akiyama, T.; Sano, K.; Nakamura, K.; Ito, T. *Jpn. J. Appl. Phys.* **2006**, *45*, L275–L278.
(7) Glas, F.; Harmand, J. C.; Patriarch, G. *Phys. Rev. Lett.* **2007**, *99*, 146101.
(8) Johansson, J.; Wacaser, B. A.; Dick, K. A.; Seifert, W. *Nanotechnology* **2006**, *17*, S355–S361.
(9) Zhang, H. Z.; Huang, F.; Gilbert, B.; Banfield, J. F. *J. Phys. Chem. B* **2003**, *107*, 13051–13060.
(10) Persson, A. I.; Larsson, M. W.; Stenström, S.; Ohlsson, B. J.; Samuelson, L.; Wallenberg, L. R. *Nat. Mater.* **2004**, *3*, 677–681.
(11) Magnusson, M. H.; Deppert, K.; Malm, J. O.; Bovin, J. O.; Samuelson, L. *Nanostruct. Mater.* **1999**, *12*, 45–48.
(12) Karlsson, L. S. Transmission Electron Microscopy of III-V Nanowires and Nanotrees. PhD Thesis, Lund University, Lund, Sweden, 2007.
(13) Kikuchi, S. *Jpn. J. Phys.* **1928**, *5*, 23.
(14) Johansson, J.; Karlsson, L. S.; Svensson, C. P. T.; Mårtensson, T.; Wacaser, B. A.; Deppert, K.; Samuelson, L.; Seifert, W. *Nat. Mater.* **2006**, *5*, 574–580.
(15) The resolution of the TEM does not allow us to resolve the closest lying atoms in the ⟨1̄10⟩ viewing direction. Therefore, the layers observed in the HRTEM images correspond to aB, bC, and cA, with the notation of Figure 3. Thus, the statistical evaluations are based on this equivalent stacking description.
(16) *Imperfections in Crystals*;. van Bueren, H. G., Ed.; North Holland: Amsterdam, 1960.
(17) Davidson, F. M.; Lee, D. C.; Fanfair, D. D.; Korgel, B. A. *J. Phys. Chem. C* **2007**, *111*, 2929–2935.
(18) Kolmogorov, A. N. *Izv. Acad. Nauk SSSR, Ser. Fiz.* **1937**, *1*, 355.
(19) Johnson, W. A.; Mehl, P. A. *Trans. AIME* **1939**, *135*, 416.
(20) Avrami, M. *J. Chem. Phys.* **1939**, *7*, 1103.
(21) Avrami, M. *J. Chem. Phys.* **1940**, *8*, 212.
(22) Avrami, M. *J. Chem. Phys.* **1941**, *9*, 177.
(23) Sear, R. P. *J. Phys.: Condens. Matter* **2007**, *19*, 466106.
(24) *Crystal Growth For Beginners*; Markov, I. V. Ed.; World Scientific: Singapore, 2003.
(25) Predel, B. In *Physical Chemistry: Phase Equilibria, Crystallographic and Thermodynamic Data of Binary Alloys*; Madelung, O., Ed.; Landolt-Börnstein: Numerical Data and Functional Relationships in Science and Technology - New Series, Group IV; Springer: Berlin, 1998; Vol. 5a.
(26) Voronkov, V. V. *Sov. Phys.-Crystallogr.* **1973**, *17*, 807–813.
(27) Hurle, D. T. J. *J. Cryst. Growth* **1995**, *147*, 239–250.
(28) Gottschalk, H.; Patzer, G.; Alexander, H. *Phys. Stat. Sol., A* **1978**, *45*, 207–217.
(29) Molenbroek, A. M.; ter Horst, G.; Frenken, J. W. M. *Surf. Sci.* **1996**, *365*, 103–117.
(30) Buffat, P.; Borel, J. P. *Phys. Rev. A* **1976**, *13*, 2287–2298.

CG800270Q